

ESI

Solvent-assisted mechanochemical crystallization of metal-free perovskite solid solution (H_2dabco , H_2hmta) $\text{NH}_4(\text{BF}_4)_3$

Jumpei Moriguchi,^a Tomoe Koga,^b Nao Tsunoji,^c Sadafumi Nishihara,^c Tomoyuki Akutagawa,^d Atsuko Masuya-Suzuki^{a,b} and Ryo Tsunashima^{*a, b}

a. *Graduate School of Sciences and Technology for Innovation, Yamaguchi University, Yoshida 1677-1, Yamaguchi, 753-8512, Japan.*

b. *Chemistry Course, Faculty of Science, Yamaguchi University, Yoshida 1677-1, Yamaguchi, 753-8512, Japan.*

c. *Graduate School of Advanced Science and Engineering, Hiroshima University, Higashi-Hiroshima 739-8526, Japan.*

d. *Institute of Multidisciplinary Research for Advanced Materials (IMRAM), Tohoku University, Sendai 980-8577, Japan.*

1. Measurements

2. h-BF_4

2.1 Preparation and characterization

2.2 SC-XRD

2.3 TG-DTA

2.4 DSC

2.5 Temperature and frequency dependence of complex permittivity

3. Solid solution crystallized from solution

3.1 Sample preparation

3.2 LC-MS

3.3 P-XRD

4. Solid solution crystallized by mechanochemical method

4.1 Sample preparation

4.2 P-XRD

4.3 TG-DTA and DSC

4.4 Temperature and frequency dependence of complex permittivity

4.5 Solid-state ^{13}C -NMR

1. Measurements

SC-XRD: Single-crystal X-ray structure analysis was performed using a Rigaku XtaLAB Synergy-DW diffractometer with a HyPix-6000HE detector (X-ray source: Mo K α). The structure was solved with the ShelXT 2018/2 structure solution program using the Intrinsic Phasing solution method and by using Olex1.5 as the graphical interface. The model was refined with a version of ShelXL 2018/3 using Least Squares minimisation. Further details of the crystallographic analysis are summarised in the CIF files deposited at the CCDC.

Temperature, K	CCDC number
112	2347881
401	2347882

P-XRD: Powder X-ray diffraction was performed using a Rigaku Mini Flex 600 at 2θ of 5-50° (X-ray source: Cu K α , room temperature). Lattice constants were calculated by Whole Powder Pattern Fitting of the diffraction patterns (PDXL 2).

CHN Elemental Analysis: CHN Elemental Analysis was performed using a MICRO CORDER JM 10.

FT-IR spectroscopy: FT-IR spectra were obtained by the transmission method using KBr disks on an instrument of Thermo Fisher Scientific avatar 370.

LC-MS: LC-MS measurement was performed using a Thermo Fisher Orbitrap Exploris 120.

TG-DTA: Thermogravimetry measurement was performed using a Rigaku TG-DTA 8122 under an Ar gas flow. The sweep rate was 10 K/min.

DSC: Differential scanning calorimetry measurement was performed using Rigaku Thermo plus EVO2 under an N₂ gas flow. The sweep rate was 5 K/min.

Complex permittivity: Complex dielectric constant measurement was performed using the E4980AL Precision LCR Meter instrument under vacuum. Measurements were made on pellet samples, with silver paste as an electrode and gold wire as electrical contacts. The typical applied AC voltage was 2 V, and the frequency range was 100 Hz to 1 MHz.

Solid state ¹³C-NMR: Solid state DD-MAS ¹³C-NMR (150.872 MHz) measurements were performed using NMR Varian 600 with a 3.2 mm diameter at 20 kHz. The chemical shift reference was hexamethylbenzene.

2. h-BF₄

2.1 Preparation and characterization

Aqueous solution of HBF₄ (3.2 ml, 20 mmol) was poured on the mixed solid of hmta (1.402 g, 10 mmol) and NH₄BF₄ (10 mmol). The mixture was then dissolved in 10 ml of hot water (90°C) and left in a refrigerator at 0°C. After 40 min, colorless block single crystals were obtained at the bottom of the flask (Figure S2-1; 0.649 g, yield 15.8 %). Elemental Anal (%): Calc C 17.12, H 4.31, N 16.69 for ((C₆H₁₄N₄)(NH₄)(BF₄)₃); found: C 17.007, H 4.232, N 16.393. FT-IR spectrum was shown in Figure S2-2.



Figure S2-1. Photograph of h-BF₄ crystals.

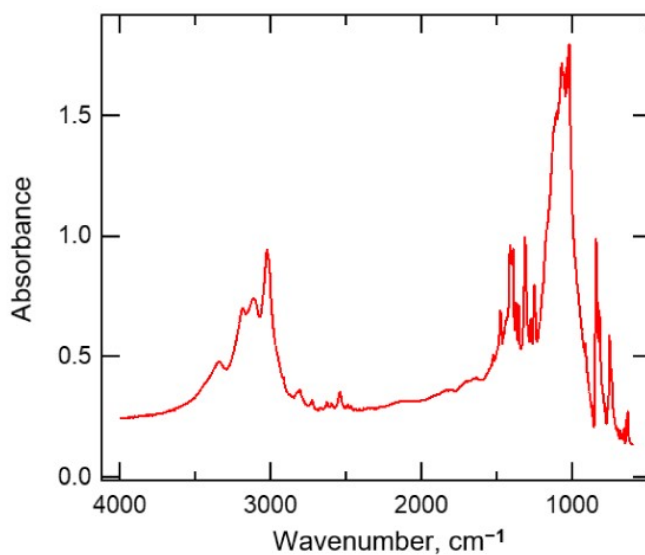


Figure S2-2. FT-IR spectrum of h-BF₄.

2.2 SC-XRD

Table S2-1 summarized crystallographic data of h-BF₄ measured at 112 K and 401 K. Figure S2-3 and S2-4 show the thermal ellipsoid view of h-BF₄ at 112 K and 401 K, respectively. The A-site molecule H₂hmta²⁺ at 401 K is randomly oriented and atoms of C and N are indistinguishable. Therefore, the structure was optimized by assuming that all are C and the free occupancy.

Table S2-1. Crystallographic data of h-BF₄

Compound	h-BF ₄	
Formula	C ₆ H ₁₈ N ₅ B ₃ F ₁₂	
T, K	112	401
C.S.	Tetragonal	Cubic
S.G.	<i>I4₁/a</i>	<i>Fm-3c</i>
<i>a</i> , Å	14.3261(2)	14.6769(8)
<i>c</i> , Å	28.6549(8)	-
<i>V</i> , Å ³	5881.0(2)	3161.6(5)
<i>Z</i>	16	8
ρ_{calc} , g cm ⁻³	1.901	1.694
Reflections collected	30780	2215
Independent reflections	2998	159
Data/restraints/parameters	2998/0/249	159/0/18
Goodness of fit on F ₂	1.061	2.253
Final R indices [<i>I</i> ≥ 2σ(<i>I</i>)]	<i>R</i> ₁ = 0.0301 <i>wR</i> ₂ = 0.0843	<i>R</i> ₁ = 0.1291 <i>wR</i> ₂ = 0.4364
Final R indices [all data]	<i>R</i> ₁ = 0.0347 <i>wR</i> ₂ = 0.0874	<i>R</i> ₁ = 0.1368 <i>wR</i> ₂ = 0.4584

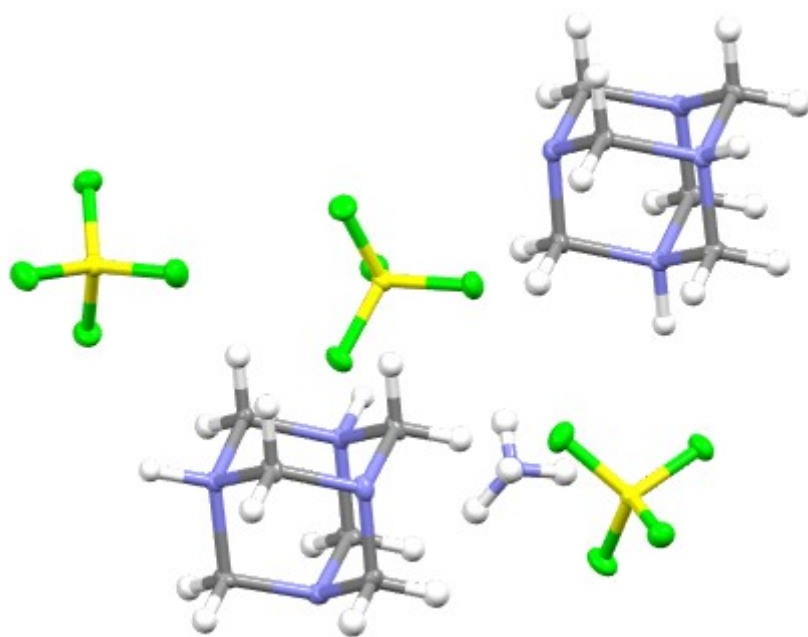


Figure S2-3. Thermal ellipsoid view (50%) of **h-BF₄** in *I*₄/*a* (Color code: gray, C; white, H; blue, N; yellow, B; green, F).

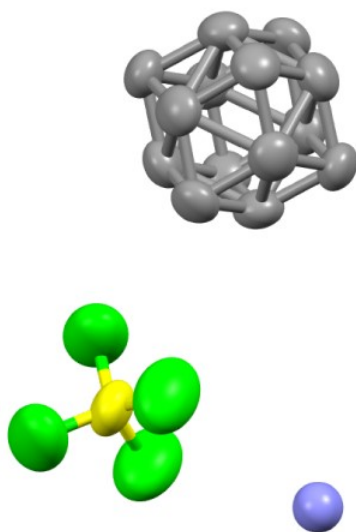


Figure S2-4. Thermal ellipsoid view (50%) of **h-BF₄** in *Fm*-3*c* (Color code: gray, C; white, H; blue, N; yellow, B; green, F).

2.3 TG-DTA

TG-DTA of **h-BF₄** was performed from room temperature to 600 K

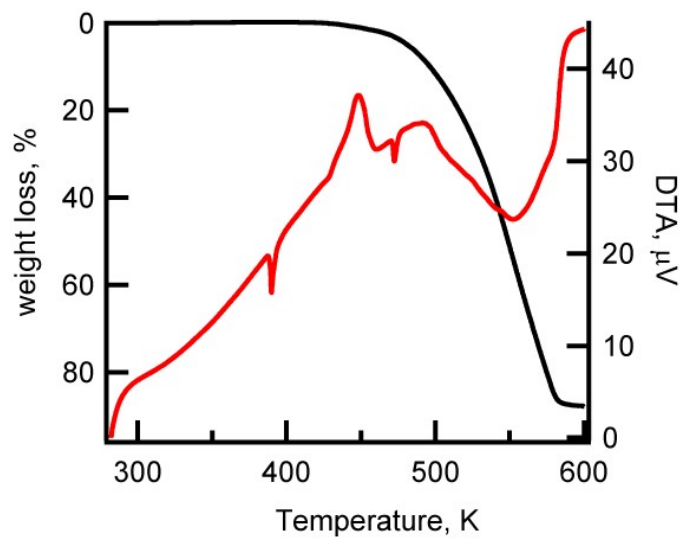


Figure S2-5. TG-DTA of **h-BF₄** at 10 K/min (colour code; red, DTA(μV); black, weight loss (%)).

2.4 DSC

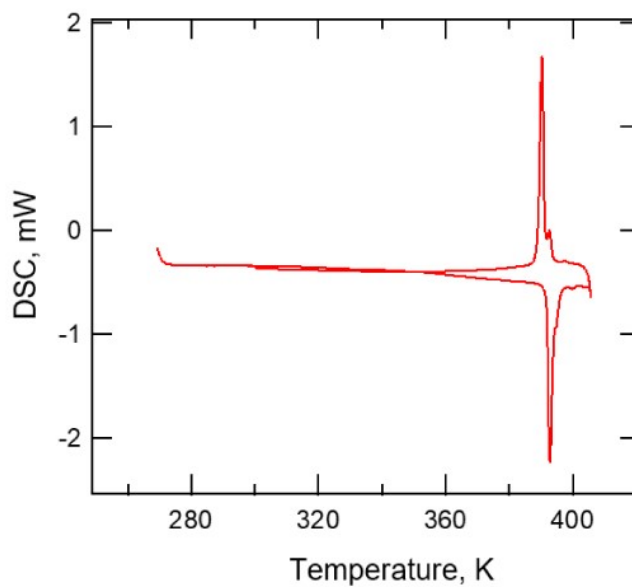


Figure S2-6. DSC of **h-BF₄**.

2.5 Temperature and frequency dependence of complex permittivity

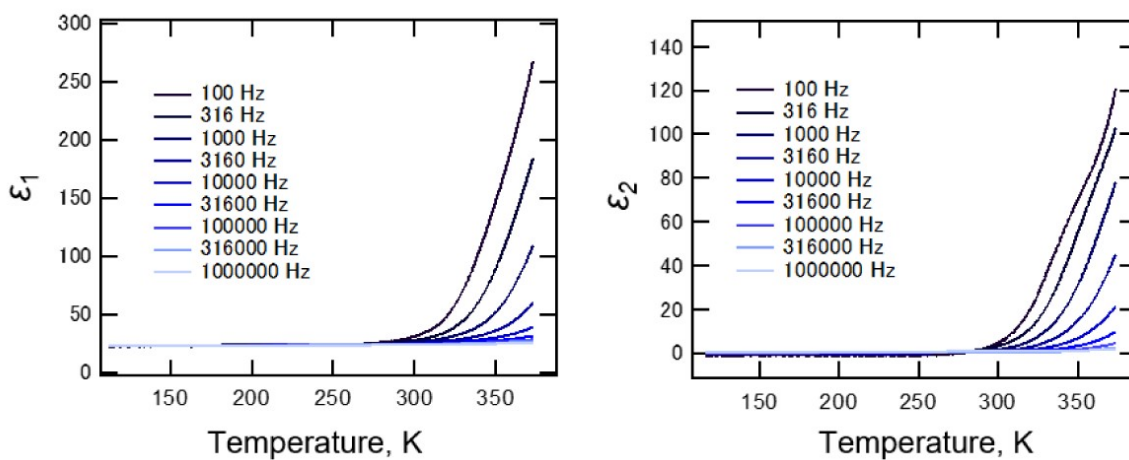


Figure S2-7. Real part (left) and imaginal (right) part of complex permittivity of h-BF_4 at 110-370 K.

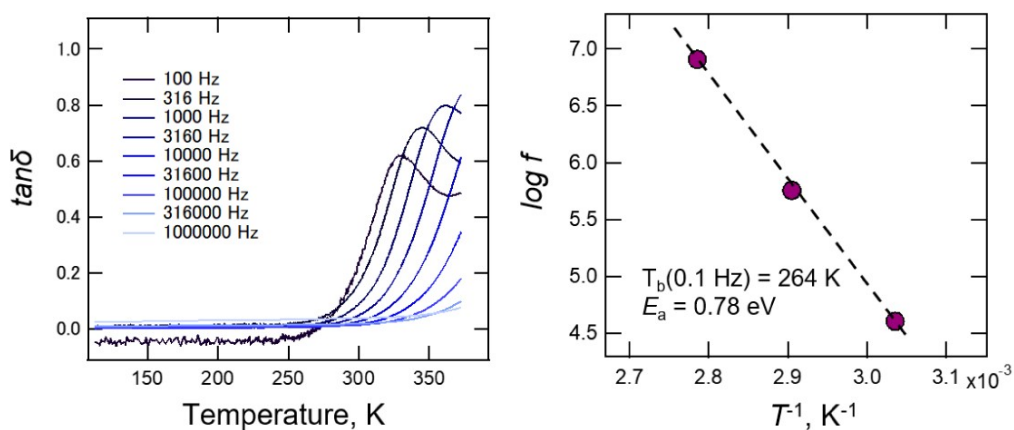


Figure S2-8. Tangent delta of a complex permittivity of h-BF_4 (left) and Arrhenius plots (right) of peak top temperatures and frequencies.

3. Solid solution crystallized from solution

3.1 Sample preparation

Aqueous solution of HBF_4 (3.2 ml, 20 mmol) was poured on the solid of mixing dabco (10 x mmol), hmta (10(1 - x) mmol) and NH_4BF_4 (7.5 mmol). The mixture was then dissolved in y ml of water at about 90°C and left to stand in a refrigerator at 0°C . After t min, colourless block single crystals were obtained at the bottom of the flask.

Table S3-1. Amount of water added V, crystallization time t, and yield %.

	V ml	t min	yield %
x = 0.1	25	15	8.70
x = 0.3	25	15	22.5
x = 0.5	20	25	21.2
x = 0.7	20	25	7.02
x = 0.9	15	30	2.92

3.2 LC-MS

Composition y (dabco: hmta = 1-y: y) was determined by LC-MS measurements. Peak intensity of for m/z for Hdabco⁺ and Hhmta⁺ were plotted by varying concentration of aqueous solution of dabco and hmta in Figure S3-1. Peak intensities were in linear relationship with concentrations, where correlation coefficient values r^2 are 0.998, and 0.997, respectively. With these linear relationships, concentrations of dabco and hmta in solid-solutions were determined.

Figure S3-2 is a plot of mixing ratio x against solid solution ratio y prepared by recrystallization menthined above. from LC-MS measurement. The composition y values at mixing ratios x = 0.5, 0.7, 0.9 were y = 0.01, 0.03, 0.24, respectively. The compositions at x = 0.1 and 0.3 were not determined due to weak peak intensity. PXRD patterns were shown in Figure S3-3. Patterns well agree with that of perovskite structures. Diffractions at x = 0.9 well agree with those of cubic phase similar to x = 0.5 prepared by mechanochemical method.

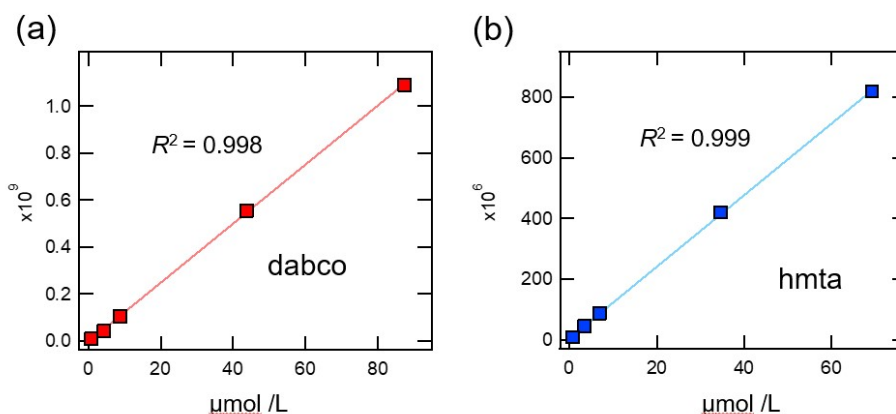


Figure S3-1. Calibration curves of (a) dabco and (b) hmta.

Table S3. CHN elemental analysis of (d-h)-BF₄.

x	y	Elemental Anal (%)	
		Calculated	Found
0.1	*a	C 18.351, H 4.602, N 10.704	C 18.436, H 4.268, N 10.827
0.3	*a	C 18.351, H 4.602, N 10.704	C 18.497, H 4.203, N 10.862
0.5	0.010	C 18.338, H 4.617, N 10.770	C 18.495, H 4.308, N 10.903
0.7	0.032	C 18.309, H 4.610, N 10.909	C 18.565, H 4.273, N 11.004
0.9	0.20	C 18.097, H 4.557, N 11.942	C 18.354, H 4.440, N 12.032

*a, below measurement range

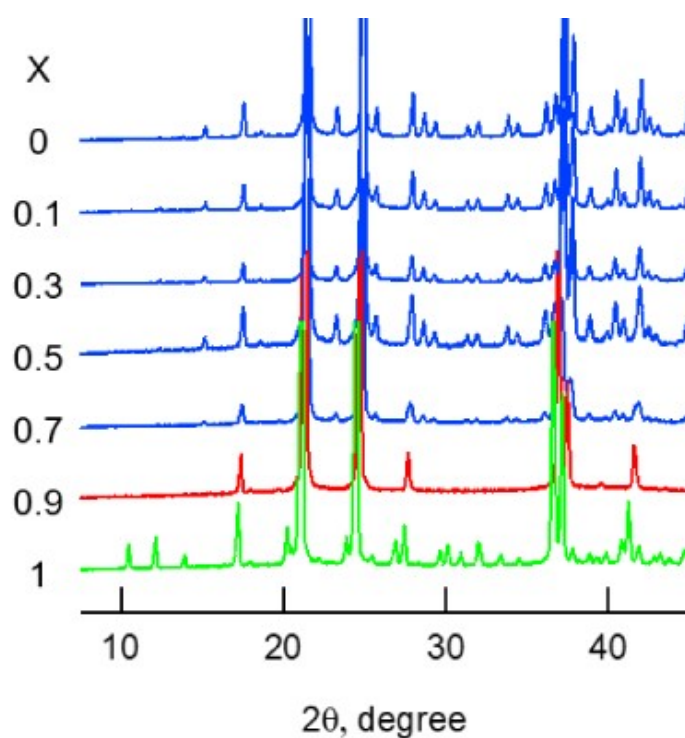


Figure S3-3. (a) P-XRD patterns at room temperature of solid solutions prepared by solution methods.

4. Solid solution by mechanochemical method

4.1 Sample preparation

A mixture of dabco (10 - 10x mmol), hmta (10x mol), NH_4BF_4 (10 - 5x mmol), and an aqueous solution of HBF_4 (20 mmol) was ground in a mortar, where 2~2.5 ml of acetonitrile was added every 5 min. After 25 ~ 30 min of grinding, the product was washed with acetonitrile and filtered by suction, and a colourless powdery solid was obtained ($x = 0.1, 0.3, 0.5, 0.7, 0.9$).

Table S4-1. CHN elemental analysis of **(d-h)-BF₄**.

x	y	Elemental Anal (%)	
		Calculated	Found
0.1	0.03	C 18.310, H 4.610, N 10.905	C 18.486, H 4.374, N 10.988
0.3	0.15	C 18.156, H 4.572, N 11.655	C 18.359, H 4.380, N 11.700
0.5	0.18	C 18.116, H 4.561, N 11.851	C 18.127, H 4.249, N 11.942
0.7	0.43	C 17.780, H 4.483, N 13.366	C 17.995, H 4.208, N 13.336
0.9	0.87	C 17.277, H 4.350, N 15.933	C 17.818, H 4.145, N 15.956

4.2 P-XRD

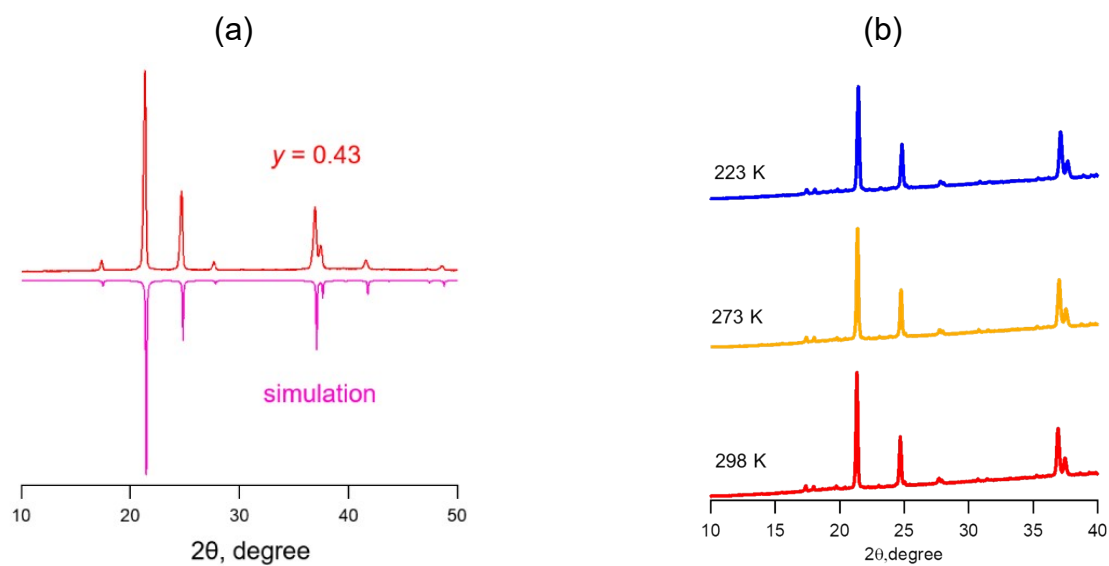


Figure S4-1. (a) Comparison of simulated and P-XRD patterns from single crystal X-ray structure analysis of **d-BF₄** in the *Fm-3c* phase. (b) Temperature dependence of P-XRD of $y = 0.43$.

4.3 TG-DTA and DSC

Table S4-2. Summary of thermodynamic values for phase transitions.

x	y	T_2 , K		ΔH , kJ/mol	ΔS , J/mol K	$\Delta H(y)$, kJ/mol	T_1 , K
		DTA	DSC	DSC	DSC	simulation	DTA
0	0	330.1	332.4	7.71	23.2	7.71	450.2
0.1	0.03	325.2	327.6	6.37	19.4	7.66	446.1
0.3	0.15	321.4	322.9	4.59	14.2	7.47	442.8
0.5	0.18	309.1	274.0(*b)	3.66 (*b)	13.4	7.42	439.6
0.7	0.43	*a	*a	*a	-	7.02	431.7
0.9	0.87	358.1	362.0	1.29	3.6	6.31	*c
1	1	388.0	392.0	6.11	15.6	6.11	*c

*a, no peak in charts; *b, very broad peaks; *c decomposed before transition

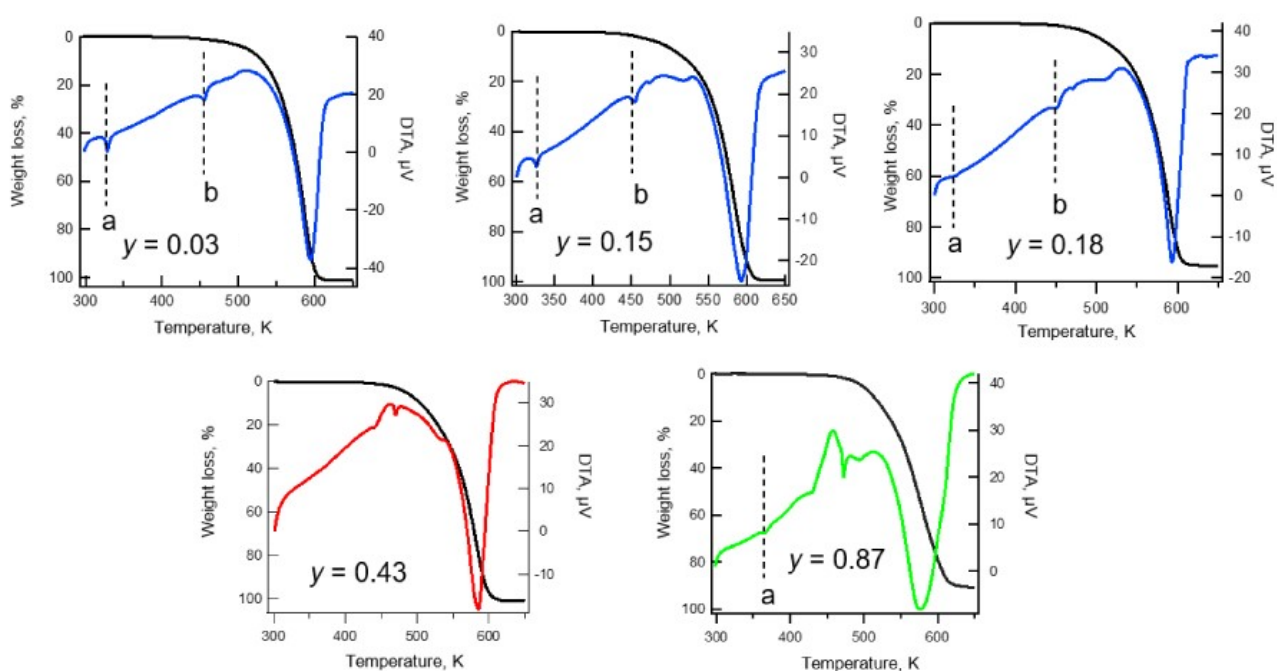


Figure S4-2. TG-DTA of $y = 0.03, 0.15, 0.18, 0.43$ and 0.87 where a and b in DTA chart represent phase transition temperature summarized in Table S4-2 (DTA: blue, red and green and TG: black).

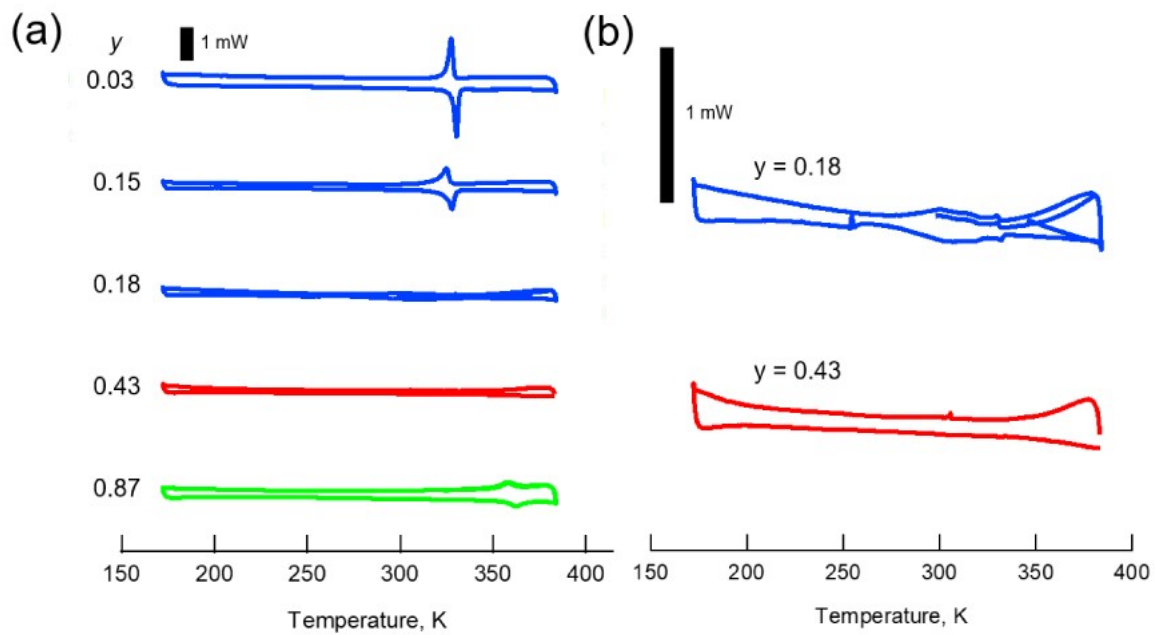


Figure S4-3. DSC of $y = 0.03, 0.15, 0.18, 0.43$ and 0.87 .

4.5 Temperature and frequency dependence of complex permittivity

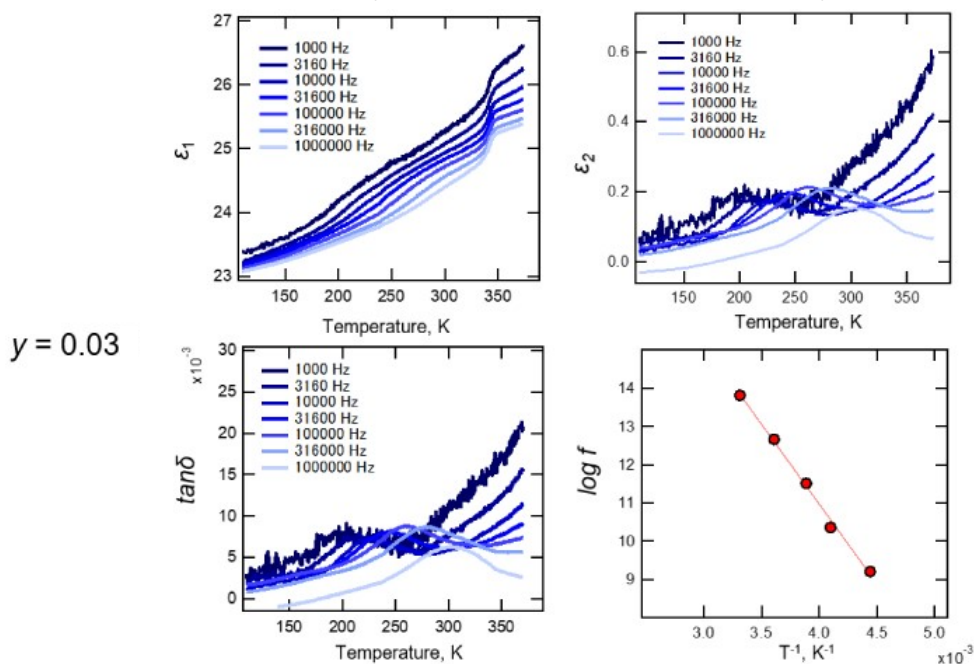


Figure S4-4. Real part (left-upper) and imaginal part (right-upper) tangent delta (lower left) of the complex permittivity at 100-370 K, and Arrhenius plots (right-lower) for relaxation of $y = 0.03$.

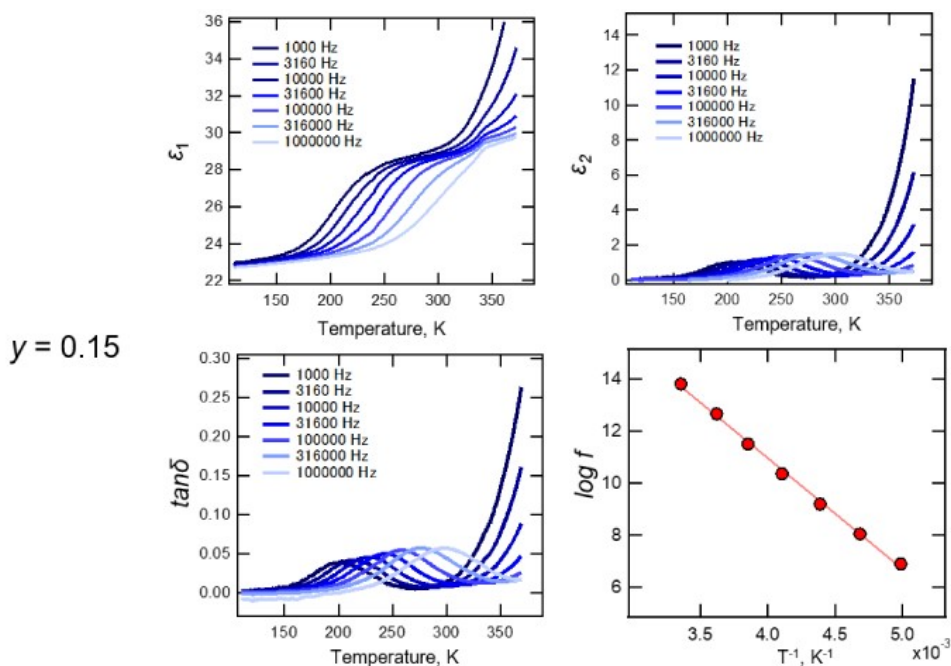
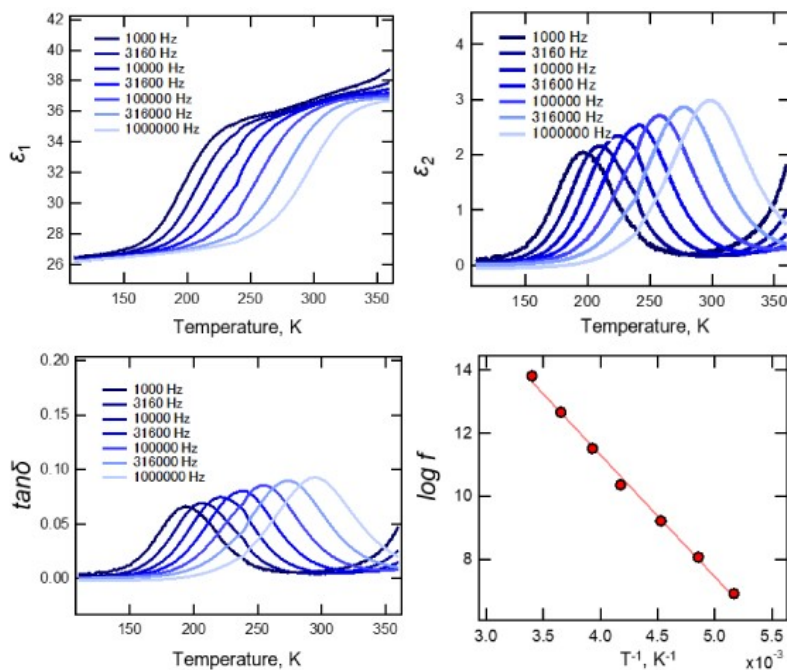
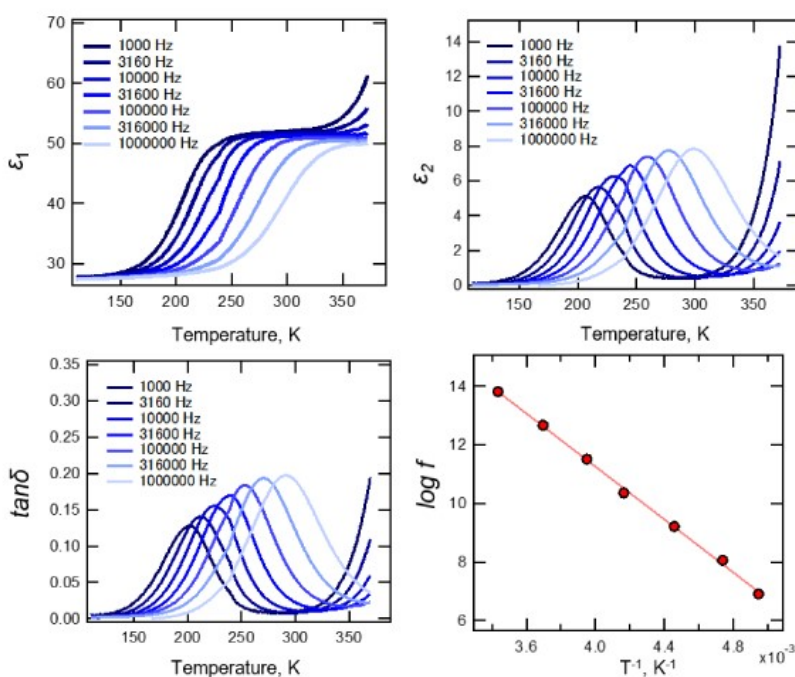


Figure S4-5. Real part (left-upper) and imaginal part (right-upper) tangent delta (lower left) of the complex permittivity at 100-370 K, and Arrhenius plots (right-lower) for relaxation of $y = 0.15$.



$y = 0.18$

Figure S4-6. Real part (left-upper) and imaginal part (right-upper) tangent delta (lower left) of the complex permittivity at 100-370 K, and Arrhenius plots (right-lower) for relaxation of $y = 0.18$.



$y = 0.43$

Figure S4-7. Real part (left-upper) and imaginal part (right-upper) tangent delta (lower left) of the complex permittivity at 100-370 K, and Arrhenius plots (right-lower) for relaxation of $y = 0.43$.

$y = 0.87$

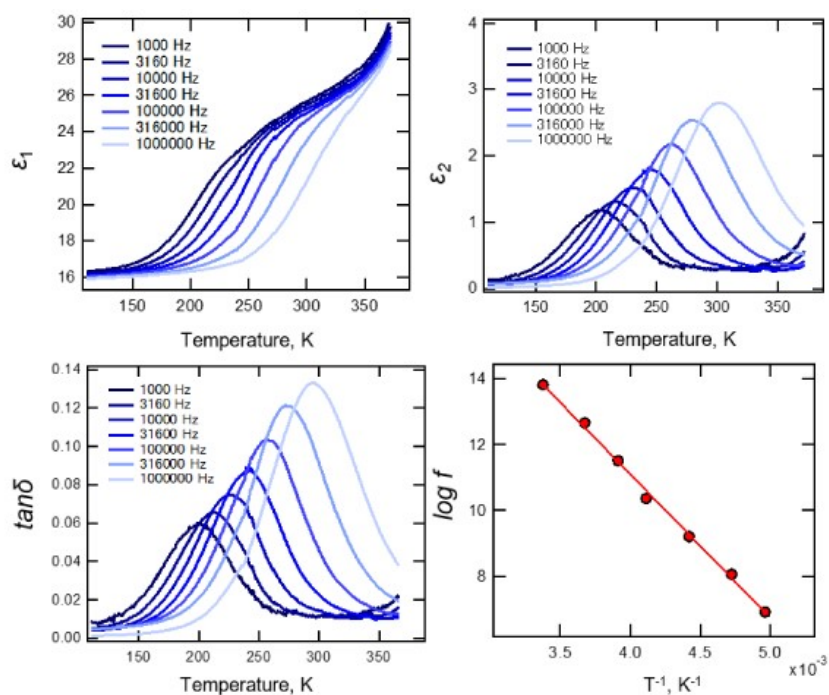


Figure S4-8. Real part (left-upper) and imaginal part (right-upper) tangent delta (lower left) of the complex permittivity at 100-370 K, and Arrhenius plots (right-lower) for relaxation of $y = 0.87$.

4.6 Solid-state ^{13}C -NMR

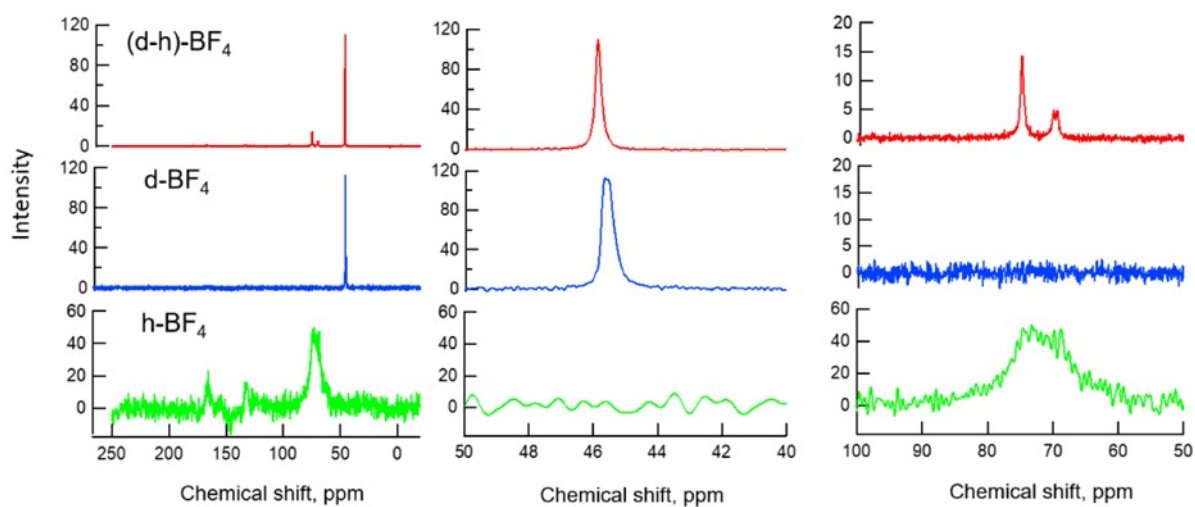


Figure S4-9. ^{13}C -NMR of $(d-h)\text{-BF}_4$, $d\text{-BF}_4$ and $h\text{-BF}_4$ at 300 K.

Table S4-1. Summary of NMR data, peak (half-width) in ppm at 300 K.

	hmta		dabco
$y = 0.43$	74.7 (0.58)	69.4 (0.64, 0.47)	45.8 (0.21)
d-BF₄	-	-	45.6 (0.39)
h-BF₄	Broad peak at 65-80 ppm		-